Fermilab FERMILAB-CONF-07-638-E

Accelerator-Based Neutrino Oscillation Experiments

Deborah A. Harris

Fermi National Accelerator Laboratory, Batavia, Illinois USA

1 Introduction

Neutrino oscillations were first discovered by experiments looking at neutrinos coming from extra-terrestrial sources, namely the sun (Fukuda et al. 1998*b*) and the atmosphere (Fukuda et al. 1998*a*), but we will be depending on earth-based sources to take many of the next steps in this field. This article will describe what has been learned so far from accelerator-based neutrino oscillation experiments, and then describe very generally what the next accelerator-based steps are. In section 2 the article will discuss how one uses an accelerator to make a neutrino beam, in particular, one made from decays in flight of charged pions. There are several different neutrino detection methods currently in use, or under development. In section 3 these will be presented, with a description of the general concept, an example of such a detector, and then a brief discussion of the outstanding issues associated with this detection technique. Finally, section 4 will describe how the measurements of oscillation probabilities are made. This includes a description of the near detector technique and how it can be used to make the most precise measurements of neutrino oscillations.

1.1 What we know so far from accelerators

The first accelerator-based neutrino oscillation experiments were designed to look for oscillations in the neutrino sector that were assumed to be similar to quark mixing: that is, very small mixing angles. CHORUS (Eskut et al. 2007) and NOMAD (Astier et al. 2001) are two recent such experiments that found no oscillations between muon neutrinos and tau neutrinos at high mass squared splittings (in other words, the two mass eigenstates would have squared mass differences, $m_1^2 - m_2^2 = \Delta m^2$ above 1 eV^2), and set limits on the oscillation probabilities at the sub per cent level. Accelerator-based neutrino oscillation experiments have also provided confirmation of the "atmospheric neutrino anomaly". They have unambiguously measured the disappearance of muon neutrinos which would correspond to a squared mass splitting of $3 \times 10^{-3} eV^2$. The two experiments that have

provided these measurements so far are K2K (Aliu et al. 2005) and MINOS (Michael et al. 2006), and at the time of this writing the mass splitting is just starting to be known well enough that results are being plotted on linear scales rather than on logarithmic scales.

The accelerator-based LSND experiment has reported evidence of muon to electron transitions at a large mass splitting ($0.1eV^2$), and this would assuredly have to be confirmed or refuted by another accelerator-based neutrino experiment (Athanassopoulos et al. 1996). Given the solar and the atmospheric neutrino oscillation signatures, if the LSND result were to be confirmed this would change drastically our picture of neutrinos and call into question even the number of neutrinos there are in the first place. For the remainder of this chapter we will assume there are three generations of neutrinos but the reader should keep in mind that if LSND were to be due to oscillations then the measurements that the next generation of neutrino experiments would be making would need to be completely re-evaluated in this totally new framework. At the time of this writing, the LSND signature has been excluded as being due to a simple oscillation scenario by the MiniBooNE experiment (Aguilar-Arevalo et al. 2007).

1.2 What is next to learn?

In the three-generation neutrino model, the mass and flavor eigenstates are related one to the other by a three-by-three mixing matrix, defined by three mixing angles $\theta_{12}, \theta_{23}, \theta_{13}$ and a CP-violating phase is δ. If $s_{ij} = \sin\theta_{ij}, c_{ij} = \cos\theta_{ij}$, then the matrix can be parameterized in the following way (Kobayashi & Maskawa 1973):

$$U = \begin{pmatrix} 1 & 0 & 0 \\ 0 & c_{23} & s_{23} \\ 0 & -s_{23} & c_{23} \end{pmatrix} \begin{pmatrix} c_{13} & 0 & s_{13}e^{i\delta} \\ 0 & 1 & 0 \\ -s_{13}e^{-i\delta} & 0 & c_{13} \end{pmatrix} \begin{pmatrix} c_{12} & s_{12} & 0 \\ -s_{12} & c_{12} & 0 \\ 0 & 0 & 1 \end{pmatrix}$$

There are several (sometimes competing) goals of the accelerator-based neutrino oscillation program. Clearly the biggest issue in the field of oscillation physics that must be addressed is that of the number of neutrinos. We want to know whether or not sterile neutrinos, which would be needed to explain the LSND signature, exist. If in fact there are three generations of neutrinos mixing, then we already know from the solar and atmospheric neutrino experiments that two of the three mixing angles are large. There is a third mixing angle whose magnitude has not been measured, although the CHOOZ experiment has determined it to be less than about 8 degrees (Apollonio et al. 2003). If this third mixing angle is found to be non-zero then the possibility of CP-violation in the lepton sector arises. Finally, in the three-generation model, there are two possibilities for the mass eigenstates: either they are "normal" or "inverted", where "normal" means like the charged fermion sector where the mass splitting between the two heaviest fermions is much larger than the mass splitting of the two lightest.

When one starts with one flavor eigenstate and searches for other flavor eigenstates, clearly there are two oscillation frequencies, corresponding to the two independent mass differences between the three eigenstates. The relevant quantities are actually the differences between the square of the masses, and the standard notation is given by $\Delta m^2_{ij} = m^2_i - m^2_j$. For a derivation of the oscillation probabilities see reference (Fisher, Kayser

& McFarland 1999). Simply put, for a transition between two different flavors, there is a term that would be proportional to $\sin^2 \Delta m^2_{23} L/E_\nu$, a term that is proportional to $\sin^2 \Delta m^2_{12} L/E_\nu$ and two terms that are proportional to $\sin \Delta m^2_{12} L/E_\nu \times \sin \Delta m^2_{23} L/E_\nu$. These last two terms are the "interference terms" which include a CP-conserving and a CP-violating piece. For the case of $\nu_\mu \to \nu_e$ and $\bar{\nu}_\mu \to \bar{\nu}_e$, the four terms can be expressed as follows, using the above definition of the mixing matrix: Starting with the above notation, these four terms can be expressed as:

$$\begin{aligned}
P(\nu_\mu \to \nu_e) &= P_1 + P_2 + P_3 + P_4 \\
P_1 &= \sin^2\theta_{23} \sin^2 2\theta_{13} \left(\frac{\Delta_{13}}{B_\pm}\right)^2 \sin^2 \frac{B_\pm L}{2} \\
P_2 &= \cos^2\theta_{23} \sin^2 2\theta_{12} \left(\frac{\Delta_{12}}{A}\right)^2 \sin^2 \frac{AL}{2} \\
P_3 &= J \cos\delta \left(\frac{\Delta_{12}}{A}\right)\left(\frac{\Delta_{13}}{B_\pm}\right) \cos\frac{\Delta_{13} L}{2} \sin\frac{AL}{2} \sin\frac{B_\pm L}{2} \\
P_4 &= \mp J \sin\delta \left(\frac{\Delta_{12}}{A}\right)\left(\frac{\Delta_{13}}{B_\pm}\right) \sin\frac{\Delta_{13} L}{2} \sin\frac{AL}{2} \sin\frac{B_\pm L}{2}
\end{aligned}$$

where

$$\begin{aligned}
\Delta_{ij} &= \frac{\Delta m^2_{ij}}{2E_\nu} \\
A &= \sqrt{2} G_F n_e \\
B_\pm &= |A \pm \Delta_{13}| \\
J &= \cos\theta_{13} \sin 2\theta_{12} \sin 2\theta_{13} \sin 2\theta_{23}
\end{aligned}$$

and the $\pm$ signifies neutrinos or antineutrinos. G_F is the Fermi coupling constant, n_e is the electron density in the earth, L is the distance the neutrino has travelled between production and detection, and E_ν is the neutrino energy.

These four terms are shown for a single neutrino energy, baseline, and value of θ_{13} in Figure 1, but for both possible mass hierarchies and all possible values of the CP violating phase δ. If there is one experiment at one energy and baseline, it is clear that even in the presence of a very precise neutrino and antineutrino oscillation probability measurement, one cannot completely determine the CP violating phase or the mass hierarchy.

Although there are these four different terms in the oscillation probability, all of the experiments so far have been only been sensitive to one of the oscillation frequencies. In particular, the atmospheric neutrino experiments measure the θ_{23} mixing angle and the magnitude of the mass splitting Δm^2_{23}. The solar neutrino experiments measure the θ_{12} mixing angle and the mass splitting Δm^2_{12}. The last unmeasured angle is θ_{13}, and in the above parameterization it is particularly clear that if θ_{13} is non-zero then there arises the possibility of a CP-violating phase δ. But to see this difference one must be sensitive to the interference term, which means that the first two terms must not be too large. It turns out that for the transitions between muon and electron neutrinos, the mixing angle θ_{13} being small means that the "first term" in the expansion will be small, giving experiments a chance to see the interference term, and therefore CP-violation.

Two simplifications that are often described are to consider the difference divided by the sum for neutrino and antineutrino oscillations: in the absence of matter effects and

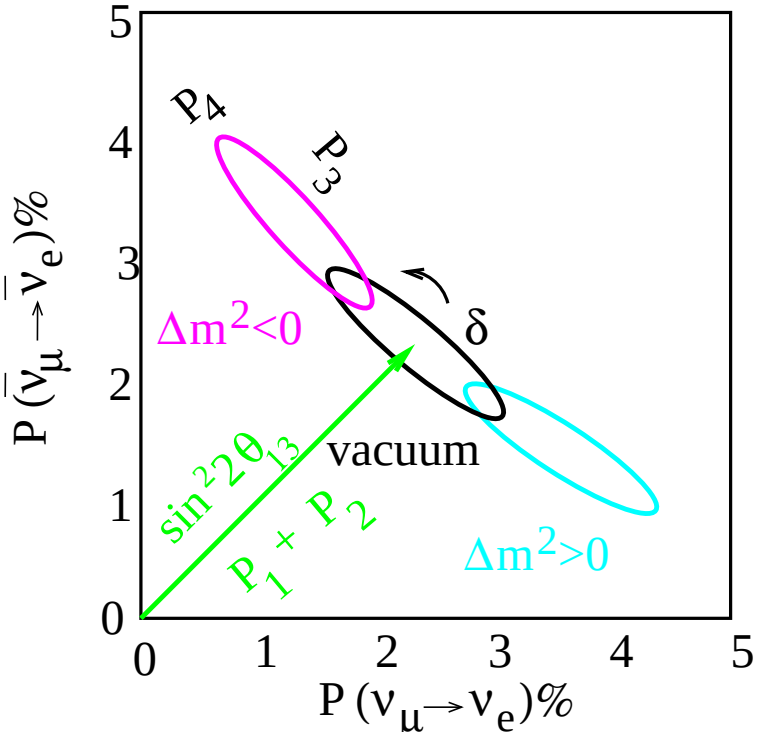

Figure 1. *Plot of the neutrino versus anti-neutrino oscillation probability for one baseline and energy. The ellipse centered on the diagonal represents the range for all possible values of δ and a given $sin^2 2\theta_{13}$ and but assuming no matter effects, and then the two other ellipses correspond to the actual ranges of possibilities for two different signs of the mass hierarchy.*

terms to second order in the solar mass squared difference:

$$\frac{P(\nu_\mu \to \nu_e) - P(\bar{\nu}_\mu \to \bar{\nu}_e)}{P(\nu_\mu \to \nu_e) + P(\bar{\nu}_\mu \to \bar{\nu}_e)} \propto \frac{\Delta m^2_{sol} L}{E} \frac{\sin\delta}{\sin\theta_{13}} \tag{1}$$

And at the other extreme, the asymmetry in the presence of matter effects at the δm^2_{23} oscillation maximum but ignoring for the moment CP violation:

$$\frac{P(\nu_\mu \to \nu_e) - P(\bar{\nu}_\mu \to \bar{\nu}_e)}{P(\nu_\mu \to \nu_e) + P(\bar{\nu}_\mu \to \bar{\nu}_e)} = \frac{2E_\nu}{E_R} \tag{2}$$

for neutrino energies below about 5 GeV, where E_R, the Earth's resonant neutrino energy, is equal to $\frac{\Delta m^2_{atm}}{2\sqrt{2}G_F n_e}$ and is ≈ 11 GeV.

The remaining sections of this article will describe some of the details of how one measures a neutrino oscillation probability using an accelerator-based neutrino source. Section 2 will describe how to make a beam of neutrinos using pion decays. Section 3 will describe the various detector technologies that are available for measuring neutrino interactions. Finally, section 4 will describe the strategies associated with making the most accurate measurements: the strategy of using near detectors, and the challenges associated with both muon neutrino disappearance measurements and electron appearance measurements.

2 Making Neutrino Beams at Accelerators

Simply put, the way to make neutrino beams at accelerators is to first make charged particles that will decay to neutrinos, magnetically focus those particles so that they are all travelling in the same direction, and then finally, give the particles a space in which to decay in flight to neutrinos. For conventional neutrino beams, the parent particles are predominantly pions, and because of the short lifetime of the pion the focused beam is simply sent through a decay volume followed by an absorber to catch the remaining particles. This results in a neutrino beam that is predominantly muon neutrino or muon antineutrino, with a small electron neutrino component that comes from kaon and muon decays. See (Kopp 2007) for a more detailed description of the techniques and challenges associated with accelerator neutrino beams, what follows here is an abbreviated summary.

A different way to make neutrino beams is from focusing and then letting decay either muons (Geer 1998) or radioactive ions (Zucchelli 2002). In both cases these particles are recirculated several times in a race-track shaped storage ring. The straight sections in the storage rings can point to one or more neutrino detectors, where the beam at the far detector is created mostly while the parent particles are decaying in those straight sections. Muon-based storage rings would provide beams that are an almost even mixture of muon neutrinos and electron anti-neutrinos (or their CP conjugates), whereas beams from radioactive ion decays, so-called "beta-beams" would be purely electron neutrino or electron anti-neutrino, depending on the ion in the storage ring. The beamline elements of these newer kinds of beams are completely different from those of conventional neutrino beams, and they will not be discussed in this article. The motivations for developing these other kinds of beamlines can be found in other proceedings at this school (Kuno 2007). In summary, the motivation is due to the fact that the fluxes can be as high or higher than conventional beams while the backgrounds can be significantly lower.

2.1 Proton Beam

The first step in producing a neutrino beam is to have an extremely intense beam of protons. Certainly the more protons in the beam, the more pions that are produced, and the number of pions produced scales as the number of protons times the proton energy, or the proton power. The requirement that these experiments look for small oscillation probabilities over very large distances has translated into enormous jumps in the required proton power to be directed towards a target in a neutrino beamline. Between the late 1990's and the early 2000's the jump in proton power has been almost a factor of 100: Table 1 shows the previous, current and next generation of proton sources and the proton power at each of these sources.

2.2 Targets

The next step in producing a neutrino beam is to put a target into the path of these protons. The longer the target, the larger fraction of protons will interact to produce pions, yet the more the produced pions will re-interact with the target either through multiple scattering or through showering. So targets for neutrino beamlines tend to be long thin objects which allow pions to exit out of the sides of the target into the focusing

Proton Source	Experiment	Proton Energy (GeV)	protons per year	Proton Power (MW)	Neutrino Energy (GeV)
KEK	K2K	12	$1 \times 10^{20}/4$	0.0052	1.4
FNAL Booster	MiniBooNE	8	5×10^{20}	0.05	1
FNAL Main Injector	MINOS	120	2.5×10^{20}	0.25	3-17
FNAL Main Injector	NOvA	120	6×10^{20}	1	3-17
CERN	OPERA	400	0.45×10^{20}	0.12	25
J-PARC	T2K	40-50	11×10^{20}	0.75	0.77

Table 1. *Comparison of proton sources: their energies, proton powers, and associated oscillation experiments.*

Experiment	Target Material	Shape	Transverse Size (mm)	Length (cm)
MiniBooNE	Be	cylinder	10	70
K2K	Al	cylinder	30	66
MINOS	graphite	ruler	6.4×20	90
NOvA	graphite	ruler	> 6.4	90
CNGS	carbon	ruler	4 mm wide	200
T2K	graphite	cylinder	12-15	90

Table 2. *Comparison of different targets in use or planned to be used in oscillation experiments, including their composition, size, and shape.*

region. Another consideration which has become important in the era of these high power proton sources is the cooling of the targets themselves. If one wants to avoid having pions reinteract or multiple scatter one wants to minimize material in the surrounding area, which puts tight constraints on the cooling system. Some targets are air cooled, while others are cooled by flowing water through nearby pipes, and finally the T2K target is designed to be cooled by flowing 300 degree Kelvin helium through the target itself (Nakadaira 2005)(Fitton, M. 2006).

The general rule of thumb which seems to be applied in most target designs is that the transverse target size is roughly three times one standard deviation in the proton spot size, in order to catch a large enough fraction of the proton beam but to not introduce too much additional material for the pions to traverse. Table 2 gives a comparison of several different targets in use (or being designed) for past, current, and future oscillation experiments.

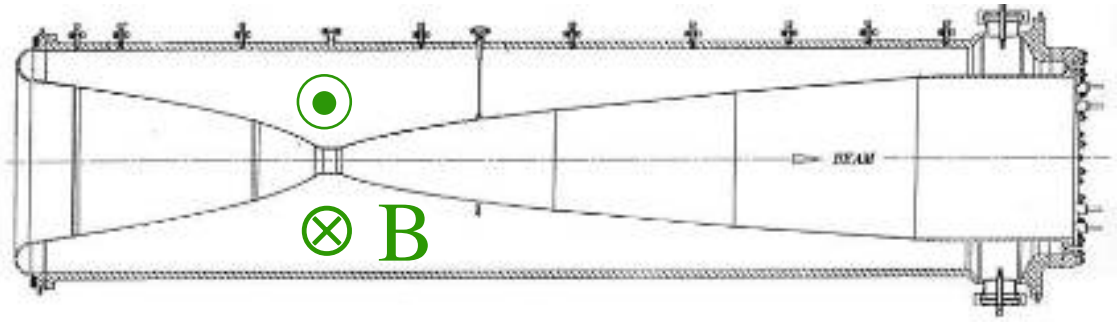

Figure 2. *Schematic diagram of a horn to focus pions coming from the left.*

2.3 Focusing Systems

The challenge of designing a focusing system for a neutrino beam is not unlike the challenge of designing a target: one wants a strong magnetic field in order to get the best focusing of the secondary particles, yet one wants to minimize the material that these secondary particles must go through. The typical transverse momentum of the pions is approximately the strong interaction energy scale, Λ_{QCD}. Although previous experiments have used alternating sets of quadrupole magnets to focus secondary particles, and solenoids have also been proposed to focus particles with a minimum of material in the path of the pions, these have the disadvantage of focusing both negative and positive pions simultaneously. This sounds like an advantage in terms of overall rate, but it would mean that in order to measure both neutrino and anti-neutrino oscillation probabilities precisely one would need to measure the charge of the final state electrons in a detector, which would be prohibitively expensive.

Consider the case of particles flying out from a single target: those particles that reach the focusing element at a higher radius are the ones with the largest transverse momentum, so they need the largest transverse momentum kick. Those particles leaving on the proton axis would need almost no transverse momentum kick. Clearly the best focusing system would be one whose integrated path length times magnetic field were proportional to the radius at which the particle entered the focusing system. The magnetic field from a line current source falls like the inverse radius, so in order to focus all the particles of a given transverse momentum, one would want the time spent in the magnetic field (or distance traversed) to be proportional to the square of the radius at which the particle entered the focusing system. This is the principle of the parabolic horn: an inner conductor is shaped in a parabola so that the length of field region at a given radius is proportional to the square of that radius, and then an outer conductor provides the return for the current. The magnetic field is completely contained between the inner and outer conductors, and there is no field at radii smaller than the inner conductor. Figure 2 shows a schematic diagram of a parabolic horn as viewed from the side (the pions enter the horn from the left in this case): note that the magnetic field is between the "horn-shaped" inner conductor and the cylindrical outer conductor. The transverse momentum kick p_t is therefore

$$\delta p_t \approx \frac{e\mu_o I}{2\pi c r} \times \frac{r^2 l}{r_{outer}^2} \approx p_{tune}\theta \tag{3}$$

where μ_0 is the permittivity of free space, I is the current in the horn, r is the average radius at which the particle traverses the horn, l is the length of the horn, and r_{outer} is

the radius of the outer conductor of the horn.

It is interesting to consider how high the current must be in a typical horn: consider two horns that are each 3 m long and 16 cm in diameter, what kind of current would be needed to give a 200 MeV/c momentum kick to the produced secondary particles?

$$\begin{aligned} \delta p_t(\mathrm{MeV/c}) &= 0.3B(\mathrm{T})l(\mathrm{m}) & (4)\\ B(\mathrm{T}) &= \frac{\mu_0 I}{2\pi r} & (5)\\ B(\mathrm{T}) &= 2\times 10^{-7}\frac{I(\mathrm{A})}{r(\mathrm{m})}(\frac{r}{r_{outer}})^2 & (6) \end{aligned}$$

And assuming that the pions would go through on average half the radius of the outer conductor, one finds

$$I(\mathrm{A}) = \frac{\delta p_t(\mathrm{GeV/c})}{0.3}\frac{2r_{max}}{l}\frac{1}{2\times 10^{-7}} \quad (7)$$

where B is the magnetic field in Tesla, l is again the length of the horn, I is the current and r is the average radius at which the particle crosses the horn.

So the currents in a horn are of the order of hundreds of thousands of Amps!

2.4 Decay Kinematics

For pions at rest, there is no preferred direction since they are spin zero particles, and they will decay isotropically. In this case the neutrino produced in the decay $\pi \rightarrow \mu\nu_\mu$ only has a single energy which is determined by the difference in the pion and muon masses. When one boosts to the lab frame, however, the neutrino energy depends on the angle between the neutrino direction in the center of mass frame and the pion boost direction which translated to the lab frame is denoted by the angle θ. It can be shown that the neutrino energy, E_ν, is related to the neutrino-pion angle (θ) and energy (E_π) in the lab frame in the following way:

$$E_\nu = E_\pi\frac{1-\frac{m_\mu^2}{m_\pi^2}}{1+\gamma^2\theta^2} \quad (8)$$

where γ is the relativistic boost of the pion, or E_π/m_π and m_μ and m_π are the muon and pion mass, respectively.

The flux of neutrinos (Φ_ν) can be derived by boosting the isotropic decays of pion at rest into the lab frame. We obtain:

$$\Phi_\nu = BR\frac{1}{4\pi L^2}\left(\frac{2\gamma}{1+\gamma^2\theta^2}\right) \quad (9)$$

where BR is the branching fraction for that 2-body decay, and L is the distance between the detector and where the pion decayed. The interesting thing to note here is how the neutrino energy increases with increasing pion energy, and the flux increases as the square of the pion energy. Given that the neutrino cross section increases linearly with neutrino energy, one would naively think that the number of muon neutrino events at a far detector simply increases as the cube of the pion energy, and as such one should try to design as high a pion beam energy as possible. However, the higher the neutrino energy, the longer

the distance one must put the far detector to probe a given mass splitting. Also, for a given incoming proton energy, the number of pions produced for a given proton energy is a steeply falling function of pion momentum. So in designing beamlines one must fold in many factors, not simply the decay kinematics.

2.5 Decay Region Strategies

As was mentioned above, there are not only pions produced when protons strike a target. Kaons are also produced, and although most of them will also undergo a two-body decay to muon neutrinos, there is a significant fraction of both charged (and neutral) kaons that will decay to electron neutrinos. This is one source of beam impurity, the other source is due to the fact that some small fraction of muons produced in pion decays will themselves decay before they reach the end of the decay region.

Suppose one wanted to design a decay region for an experiment looking for muon to electron neutrino oscillations: one would want to minimize the fraction of electron neutrinos per muon neutrino. The longer the decay region, the larger a fraction of pions that would decay, but the larger the fraction of muons that would also decay. By considering the average decay length of a beam of pions of energy E_π and calculating the fraction of muons that would decay in the remaining length of the decay pipe, one can show that the ratio of electron to muon neutrino fluxes is dependent on the decay pipe length (L), the average pion energy, and the pion and muon lifetimes:

$$\frac{\Phi(\nu_e)}{\Phi(\nu_\mu)} = \frac{L m_\mu c}{E_\pi \tau_\mu} \left(\frac{1}{e^{y_\pi} - 1} + 1 + \frac{1}{y_\pi} \right) \tag{10}$$

where y_π is the number of pion lifetimes in the decay pipe:

$$y_\pi = \frac{L m_\pi c^2}{E_\pi c \tau_\pi} \tag{11}$$

In this equation τ_i is the lifetime of particle i, m_i is the mass of particle i, and E_i is the energy of particle i in the lab frame. One can similarly define y_μ as the number of muon lifetimes in the decay pipe

$$y_\mu = \frac{L m_\mu c^2}{E_\mu c \tau_\mu} \tag{12}$$

Table 3 gives the lengths of several decay pipes of past, current, and future oscillation experiments, as well as the average pion energy and the calculated theoretical ratio of electron to muon neutrino fluxes. Keep in mind that these calculations are for the integrals of the fluxes: clearly the fluxes from 2-body decays producing muon neutrinos will be more collimated than those from the three body decays. Similarly, the neutrino energies from the two body decays carry on average a larger fraction of the pion energy than those from the three-body muon decays.

2.6 Off Axis Strategy

For the future searches for ν_μ to ν_e appearance, one wants to minimize the fraction of electron neutrinos in the beamline. One strategy might be to make the decay region very

Experiment	Length	E_π (GeV)	y_π	y_μ	$\frac{\Phi(\nu_e)}{\Phi(\nu_\mu)}$ (approx)
MiniBooNE	50m	2.5	0.36	0.3%	0.15%
K2K	200m	3.5	1.0	0.9%	0.5%
MINOS	675m	9	1.3	1.2%	0.8%
CNGS	1000m	50	0.36	0.3%	0.15%
T2K	130m	9	0.47	0.2%	0.10%

Table 3. *Decay pipe characteristics of several decay volumes of currently operating or planned neutrino beamlines. For the MINOS experiment, the beamline decay pipe parameters are defined for that experiment, while for the NOvA experiment, which uses the same beamline but a different peak of focused pion energy, y_π and y_μ will be slightly different.*

short so that there are no tertiary muon decays, another strategy might be to also make the incoming proton energy very low so that there are a minimum of kaons produced. However, both of those strategies will also reduce the muon neutrino rate at least as much as the electron neutrino rate. One technique that reduces the ratio of electron neutrinos to muon neutrinos at a given energy is to put the far detector slightly off of the pion beamline axis. For a two-body pion decay, the neutrino energy is completely determined by the pion boost and the angle between the pion momentum and the neutrino direction. Figure 3 shows the transverse versus longitudinal neutrino momentum for pions at different energies, represented by different ellipses. Note that for on-axis decays the neutrino longitudinal momentum, and hence the neutrino energy, is linear with the pion energy. This corresponds to the case in Equation 8 where θ_μ or the angle between the pion and the neutrino (detector) direction, is equal to zero. However, as the far detector angle moves slightly off axis, there is a broad range of pion energies that will contribute neutrinos in a much narrower range of neutrino energies. Because the electron neutrinos come primarily from three-body decays instead of two-body decays, this peaking in energy is not nearly as pronounced.

So although putting a far detector off the axis to which the pions are focused will reduce the peak muon neutrino energy as well as the muon neutrino rate the ratio of electron to muon neutrino fluxes drops substantially. This technique will be put to use by both the T2K and NOvA experiments to optimize their searches for ν_e appearance.

3 Detecting Neutrinos from Accelerators

In conventional neutrino beams, one has a predominantly muon neutrino beam with a small admixture of electron neutrino contamination, which will be less than a per cent for future experiments. So to measure $\nu_\mu \rightarrow \nu_e$ transitions one must first and foremost be able to distinguish between electrons and muons, but one must also be able to distinguish between electrons and neutral pions, which are made in a large fraction of neutrino interactions above several hundred MeV. Neutrino beams focused with horns are predominantly neutrinos or anti-neutrinos, depending on the polarity of the horn current, so a detector in a conventional beam does not need to identify the charge of the final state

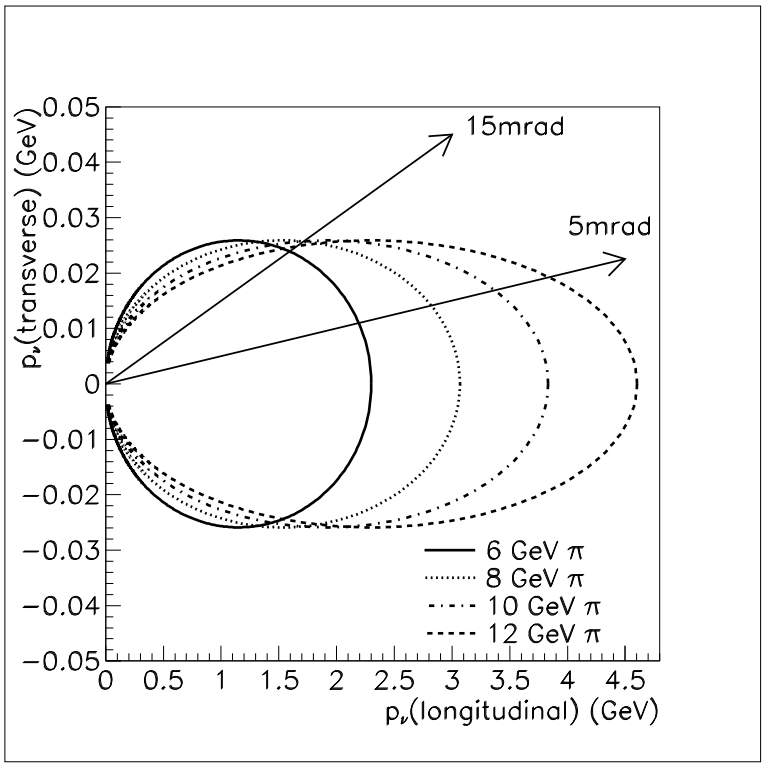

Figure 3. *Plot of the transverse versus longitudinal neutrino momenta. Different ellipses correspond to different parent pion energies. An off-axis detector located at a given angle with respect to the beamline axis will see neutrinos of energy corresponding to the intersect of that angle and the set of ellipses corresponding to the focused pion peak energies.*

lepton, merely the flavor.

Neutrino beams made from decays of beams of muons (so-called "neutrino factories") present another challenge entirely. Since the beam will have roughly equal numbers of electron neutrinos and muon antineutrinos, (or vice versa), the detector will need to again distinguish between electrons and muons, but will also need to measure accurately the charge of that final state muon: if the muon charge is the same as the charge of the muon circulating in the storage ring, it means that the muon was produced from a muon neutrino from that ring. However, if the charge of the final state muon is the opposite of the charge of the muons in the ring, then it must have come from an electron neutrino that has oscillated into a muon neutrino. When this idea was first developed it was appreciated that the probability of mis-identifying the charge of a muon could be reduced to well below the intrinsic electron neutrino contamination of a conventional beam. This means that one could have access to much lower backgrounds, which would in turn allow access to much lower mixing angles than with a conventional beam (Geer 1998).

Neutrino beams made from the decays of radioactive ions are purely electron neutrino or antineutrino, depending on the ion in the ring (Zucchelli 2002). For this reason they are the closest one could get to "preparing a beam in a flavor eigenstate". The measurement in a far detector of a muon neutrino would unambiguously signal oscillations. The challenge of these "beta-beams" is that to get above the threshold for muon neutrino charged current interactions the neutrino beam energy must be above a few hundred MeV (Burguet-Castell, Casper, Gomez-Cadenas, Hernandez & Sanchez 2004). Because the difference in

Total Detector Mass	Events Per Detector Background ν_e	NC	Total	Signal Events	Figure of Merit (Significance)
5 kton	2.5× 5	400×.0025 × 5	17.5	25	3.8
15 kton	1.5× 15	400×.005 × 15	52.5	45	4.6

Table 4. *Signal and background event calculations for the sample experiments described in the text. The neutral current rates are* 400 *events per kiloton of detector, and the* nu_μ *charged current rates are assumed to be 1000 events per kiloton of detector. The oscillation probability is assumed to be 1% in this example. The significance is defined as the signal divided by the square root of the number of signal and background events.*

total mass between the initial state and the final state of these decays is so small this means an enormous energy per nucleon would be required for a given neutrino energy. Similar to the neutrino factories, the detector challenge here would simply be to distinguish muons from electrons, and the energies would likely be low enough that not many pions would also be produced in the final state neutrino interactions.

3.1 Backgrounds

To understand why it is not only the signal rate but also the background rates which are important, consider the following two scenarios: a 5 kton detector has a 50% acceptance for ν_e charged current events, and only a 0.25% probability of mis-identifying a neutral current event as a background event. Another detector is only 30% efficienct for ν_e charged current events, and has a higher background mis-identification probability of 0.5%. But because the second detector is less fine-grained, it is significantly cheaper and for the same money one could build 15 kton of the second detector. Assume in both cases that there is also a 0.5% intrinsic ν_e component in the ν_μ beam. Which detector would see a larger signal, if the $\nu_\mu \to \nu_e$ oscillation probability were 1.0%? Assume 1000 ν_μ charged current events per kiloton, and 400 neutral current events per kiloton. If the ν_e contamination is 0.5%, then this implies 5 ν_e charged current events per kiloton as an intrinsic background (before acceptance efficiency is applied).

So although on the surface the more coarse-grained detector seems worse, by being able to build more of it one can design a more sensitive experiment, see Table 4.

Now to do the same exercise for a neutrino factory, imagine you have a factory which produces 500 (200) $\bar{\nu}_\mu$ charged (neutral) current events per kiloton, and 1000 (400) ν_e charged (neutral) current events per kiloton, and again assume a 1% oscillation probability, and a background rate of 0.1% for all kinds of interactions, and a 50% ν_μ signal efficiency and 15kton of detector (because it is less challenging than a ν_e appearance detector): The background in this case is $0.0001 \times 2100 \times 15 = 3$, while the signal events would number $1000 * 0.01 * 0.5 \times 15 = 150$, and the signal over the square root of the background would be 12 instead of only 3 or 4 in the above case. Another way of thinking of this is that the neutrino factory would see a 12 sigma result rather than a 3 or 4 sigma result.

Material	Radiation Length (cm)	Interaction Length (cm)	dE/dx (MeV/cm)	Density (g/cm^3)
Liquid Argon	14	83.5	2.1	1.4
Water	37	83.6	2.0	1
Steel	1.76	17	11.4	7.87
Scintillator (CH)	42	80	1.9	1
Lead	0.56	17	12.7	11.4

Table 5. *Summary of material properties used in neutrino detectors.*

3.2 Particles passing through Material

Before discussing the various detectors used for neutrino oscillation experiments it is worth reviewing briefly what happens when particles pass through material. Because neutrinos interact so rarely one is usually faced with using the active material in the detector as a neutrino target itself. If one is trying to search for electron neutrinos, then one would care about the detector segmentation in terms of radiation lengths. If one is looking for muon neutrinos, then the issue is more the segmentation in terms of the length of a typical muon track, which is determined by dE/dx in that material. Finally, if one is looking for a τ neutrino interaction, then the important distance to keep in mind is the decay length of a τ, which is the usually small boost of the tau multiplied by 87 microns. Table 5 gives a summary of some of the materials that are used for neutrino detectors (Yao, W.M. et al. 2006).

3.2.1 Charged Particle Energy Loss

The Bethe-Bloch equation describes how much energy per unit distance is lost as a particle traverses a medium. Energy loss is a function of the particle's charge (z), velocity normalized to the speed of light (β) and Lorentz boost (γ) of the particle, the electron mass m_e, as well as the atomic number (Z) and atomic mass (A, in units of grams per mol) of the medium in question. Because dE/dx depends on γ and β it can be used at some level for particle identification, especially if a particle ranges out in that material. The Bethe-Bloch equation is expressed as follows:

$$\frac{dE}{dx} \propto z^2 \frac{Z}{A} \frac{1}{\beta} \frac{1}{\beta^2} \left[\frac{1}{2} \frac{\ln 2m_e c^2 \beta^2 \gamma^2 T_{max}}{I^2} - \beta^2 - \frac{\delta}{2} \right] \tag{13}$$

where x is expressed in units of g/cm^2, T_{max} is the maximum kinetic energy imparted to a free electron in a single collision, and δ is a density effect correction (Yao, W.M. et al. 2006). This equation is shown for different particle species in Figure 4. Note that at high particle momenta the energy loss per unit distance is comparable for all the particle types, but that as the particles get to very low momenta (for example just before they range out) the energy loss levels are very different.

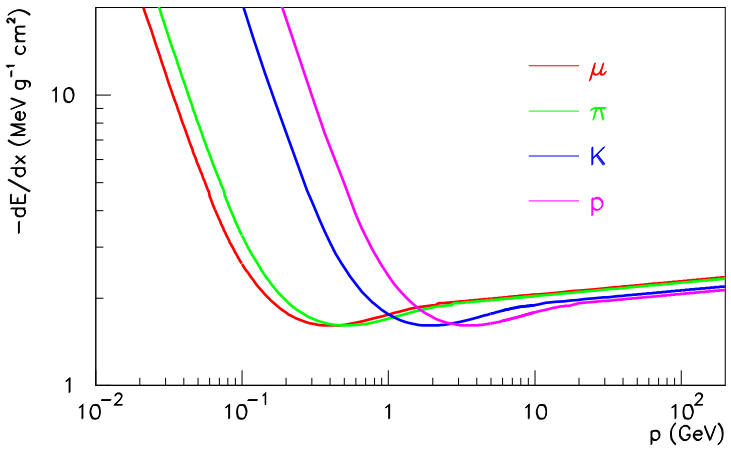

Figure 4. *Plot showing the energy loss per unit distance as a function of momentum for different particle species.*

3.3 Liquid Argon TPC

A liquid argon TPC is made by filling a vessel with ultra-pure liquid argon and 2 wire planes at right angles to each other. When an electric field is applied a charged particle that passes through the detector will ionize the Argon, and the free electrons will drift along the direction of the electric field. This will produce a signal on the planes of wires, and by measuring the signal on the two planes of wires as a function of time one can reconstruct a 3-dimensional (3-d) picture of the charged particles that produced the electrons. The higher the energy deposition the more electrons are produced, so you get not only a 3-d picture of the event, but you can use the Bethe-Bloch equation to get back to the type of particle that ionized the electrons.

Figure 5 shows this idea in practice: this is from the cosmic ray run in Pavia of a 600 Ton Liquid Argon TPC, where there is clearly a charged particle decay chain (Rubbia, A. 2005).

One promising way to discriminate between showers that originate from photons (from neutral pions) and those that originate from electrons (from electron neutrino charged current events) is to look at the first few radiation lengths of the interaction. At the very start of the interaction the dE/dx is nearly constant with momentum (see Figure 4), but a photon would convert to an electron and a positron, so the dE/dx would be twice as high for a converted photon as for an electron. By requiring all signal electrons to not start showering in the first 2 radiation lengths of material one loses only a small amount of signal and rejects all but a few per mil of the incoming π^0's, as shown in Figure 6.

At the time of this writing there are a few outstanding issues for the Liquid Argon TPC: the only downside of having so much information about each event is that the event reconstruction can be extremely challenging. The more experience the field gets with these detectors in known neutrino beams the more the reconstruction techniques can be improved. Right now there is substantial work on simulations of this kind of detector, but it is extremely important to show that the simulations agree with the actual detector performance, by using a known (neutrino) source. One very interesting possibility is that

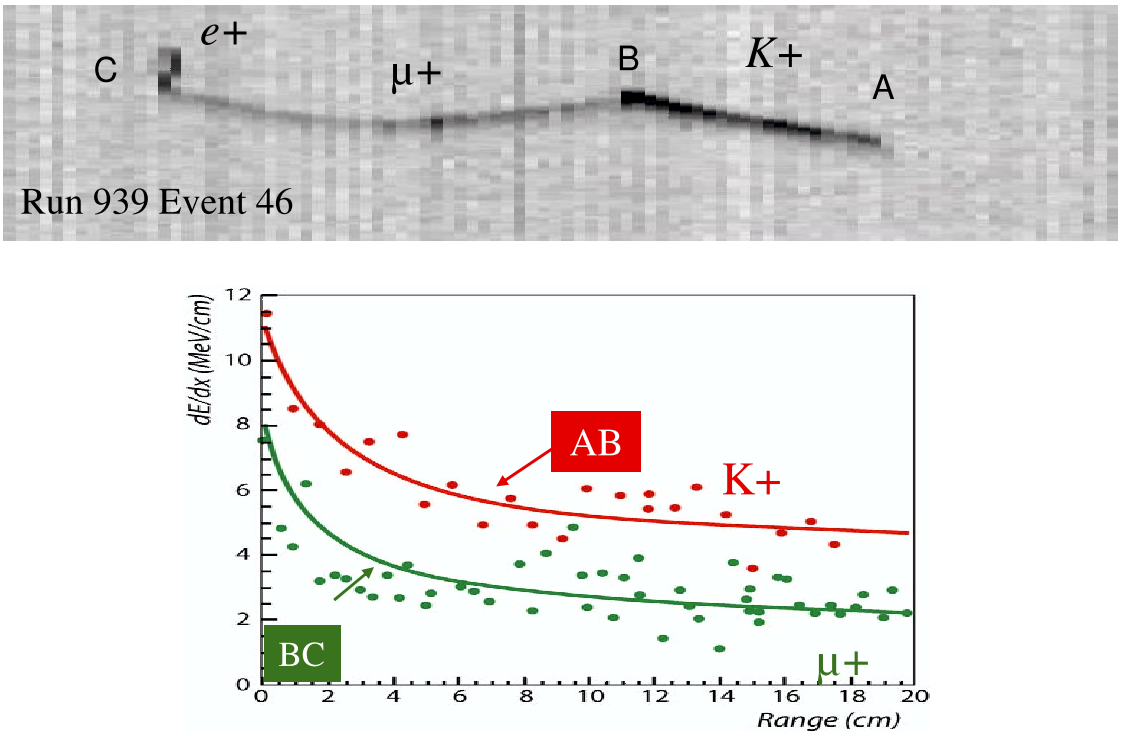

Figure 5. *An event display from a cosmic ray test run of a Liquid Argon TPC (top) and a plot of the energy deposition as a function of the distance from the end of the track (bottom). Figures courtesy of the ICARUS collaboration.*

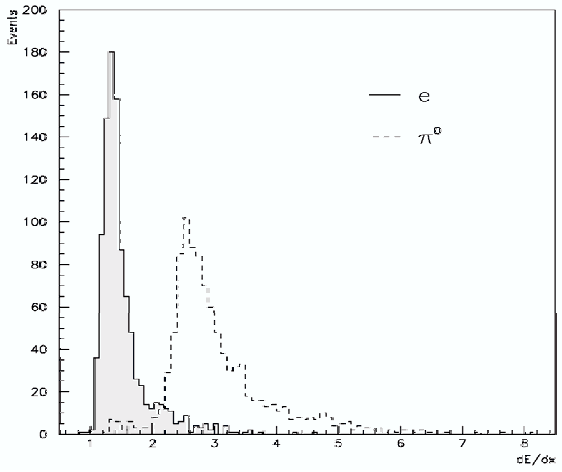

Figure 6. *The distribution of energy deposited in the first two radiation lengths of a liquid argon TPC for electrons and for photons coming from the decays of neutral pions.*

of putting one of these detectors in a magnetic field: in that way it could be used for both a conventional beam and a neutrino factory experiment and have extremely high signal acceptance.

Another issue has to do with the cost of this detector: clearly the fewer wire planes that are needed, the less expensive this detector would be. The ICARUS detector ran with wire planes separated by 1.5 m and has made Argon pure enough to use a 3 m spacing,

but if the spacing could be 5 m or longer then there would be significant cost savings. Finally, regarding the cost an important issue for most of these detector technologies is one of granularity: the finer the wire spacing the more precise the 3-d picture is. However, for accelerator-based neutrino energies it is not clear that 3 mm wire spacing is critical, and the detector would be substantially less expensive if a wider pitch could be used.

3.4 Cerenkov Detectors

As particles move faster than the speed of light in a given material, a "shock wave" of light is produced. This shock wave propagates out at the Cerenkov angle θ_c, which is defined as $\cos\theta_c = 1/n(\lambda)$ where $n(\lambda)$ is the index of refraction for the wavelength λ of the Cerenkov light in that material. For water, this angle is about 43^o. The momentum threshold for a particle to emit Cerenkov radiation is equal to the particle's mass divided by $\sqrt{n(\lambda)^2 - 1}$. Given what the index of refraction is for "typical" materials, this means that the thresholds are when particles have momenta that are roughly 35% above their rest mass.

This light is collected by phototubes placed on the edge of the active volume, and since a cone of light is produced, one only has to measure photons in enough places that one can reconstruct a circle as the cone passes through the surface of the detector.

Although this technique has very low threshold for electrons, the threshold for muons is much higher, and the thresholds for protons and pions are higher still. Nevertheless it remains an extremely powerful detector technique, because you can collect this light by putting detectors on the surface of this vessel, so the cost per unit mass is potentially lower than other techniques where one has to instrument the entire volume of a detector.

In order to determine which signals come from a given interaction, one needs the timing information associated with each phototube hit. The time of flight information is used to determine the origin of the neutrino interaction, and then all the tubes that are determined to be within a specified time window are used to find rings. A Hough Transformation (Shiozawa 1999) is used to associate given phototube hits with a set of rings. Once the rings are determined then the particle identification can begin, as well as energy reconstruction. In many cases, the decay electron coming from a stopped muon can also be found, although it will make a signal later in time than the primary muon signal.

Given the different ways in which particles interact in materials, different particles will produce different patterns of Cerenkov radiation. Therefore this technique can provide flavor information about the incoming neutrino. For example, muons can travel a long distance in material and lose energy slowly, so that means that they will produce many concentric rings of Cerenkov light before they go below threshold. Also, compared to electrons they have much less multiple scattering, so muons (and pions) will produce much sharper outer rings than electrons will produce. Electrons only go a short distance in material before producing showers and losing energy, so their rings may be brighter but have much fuzzier edges. Finally, photons are visible when they convert to an electron positron pair, and for the energies of interest those two particles are collinear, so each photon will look like a single electron-like ring. Neutral pions will decay to two photons, so depending on how large the angle is between those two photons, a neutral pion will pro-

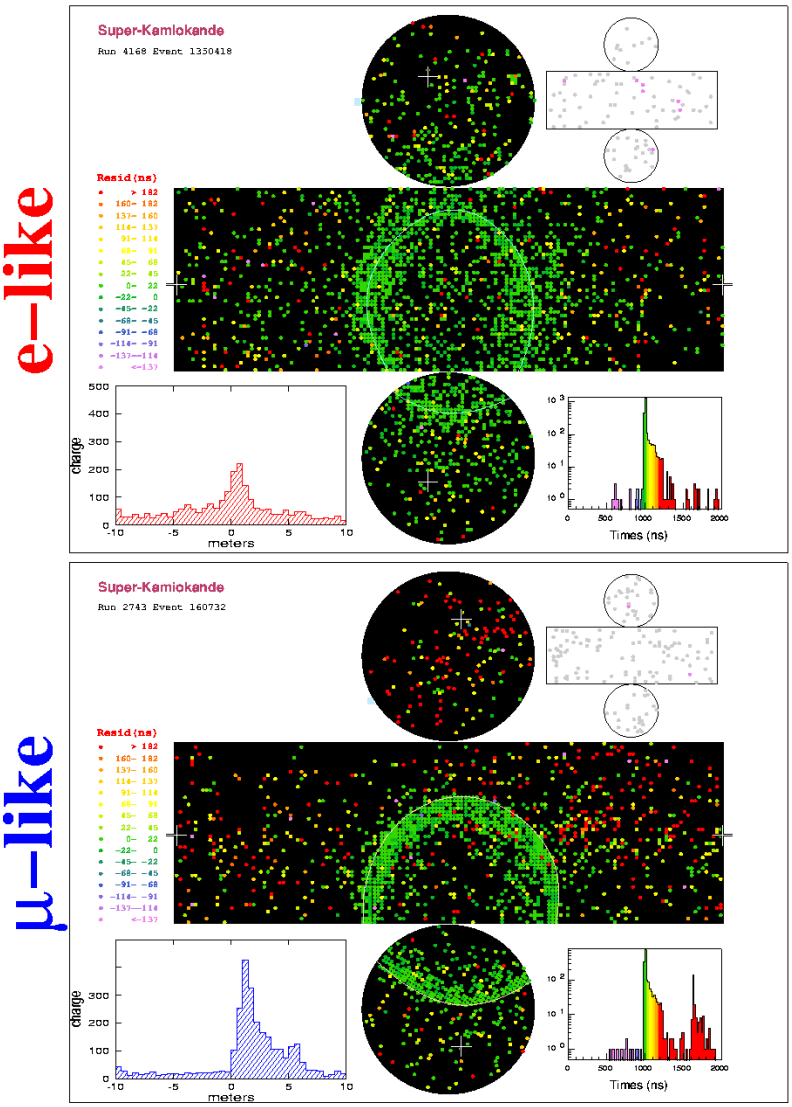

Figure 7. *Two event displays from the Super-Kamiokande Water Cerenkov Detector: one for an electron neutrino interaction (top) and one from a muon neutrino interaction (bottom). Figure courtesy of the Super-Kamiokande collaboration.*

duce two separate electron-like rings. Figure 7 shows events from the Super-Kamiokande detector (Nakahata et al. 1999) with roughly 0.5 GeV of visible energy, but one (on the top) that is produced by an electron and one (on the bottom) by a muon, respectively.

The most significant outstanding issue associated with water Cerenkov detectors is how far in size this detector technology can be extended. The largest neutrino detector to date that has been constructed, Super-Kamiokande, uses water Cerenkov technology. Making a still larger single-volume Cerenkov detector appears to be the most economical way to increase the detector mass, since one only needs to instrument the surface of the vessel rather than the volume. Eventually, however, the absorption length of water at the Cerenkov light frequencies (60 m) will limit the ultimate size of a single vessel. Also, there are concerns that the water pressure on too large a vessel would be damaging to the phototubes, so in fact more physically robust methods of collecting light over large areas

are being pursued.

Another outstanding issue associated with water Cerenkov detectors is the appropriate energy regime. Although water Cerenkov detectors have proven extremely effective at the 0.5-1.5 GeV neutrino energy regime, they have yet to be fully exploited at higher energies, where there are several rings in the detector that must be identified and analyzed. As the neutrino energy gets higher, there are more and more particles produced in the interaction: the more particles that are above Cerenkov threshold the more rings must be found, yet a larger fraction of the neutrino energy will also be lost to particles that get produced below Cerenkov threshold. Currently the Super-Kamiokande detector has 10% of the vessel's surface covered with photo-tubes; if a higher fraction were covered then more rings could be distinguished, allowing the detector to function better at higher energies. One remaining issue is that for muons that do not range out of the water Cerenkov detector, an energy measurement is not possible without an additional detector downstream. Given the absorption length of 60 m mentioned above, this translates into 12 GeV muon energy loss across the full detector, or an average of 6 GeV energy loss for particles originating in the center of the detector.

Finally, the sensitivity of phototubes to a magnetic field means that it would be extremely difficult to use this kind of detector technology in a neutrino factory experiment, where charge identification is necessary to distinguish the incoming neutrino flavor.

3.5 Sampling Detectors Overview

Another powerful technique for neutrino detector is to use sampling detectors. The benefit is that by having a significant fraction of material in the detector that is not active, there are fewer readout channels, and therefore the readout costs are lower, but also this also means that denser material can be used which would provide more detector mass in a given enclosure. By adding steel to the list of possible detectors then one can also envision large detectors that are easily magnetized, which is a requirement for a detector used at a neutrino factory. The disadvantages to sampling are of course that there is a loss of information, and particle identification is more challenging because of that loss. For a sampling detector, the energy resolution is usually dominated by the number of samples that are made in a given shower: for electromagnetic showers, the resolution scales as the square root of the samples per radiation length, while for hadronic showers it's the square root of the samples per interaction length.

It is worth noting a few differences between high atomic number and low atomic number, Z, sampling calorimeters to understand why in some cases the detector mass is made of lead or steel, while in other cases the detector mass is made of hydrocarbons. In high Z materials the electromagnetic and hadronic showers are far more compact. For example if one is trying to see small distances scales such as a kink in a $\tau \rightarrow \mu$ decay then it is natural to require a small transverse segmentation. It is also clear that the higher Z materials are far more dense than the low Z materials, so the size of the building or cavern excavation would be considerably smaller for high Z detectors.

The main advantage of the lower Z target materials is that if one considers the number of target nuclei per radiation length then low Z materials are superior. The fact that the hadronic and electromagnetic showers are far more spread out also means that the

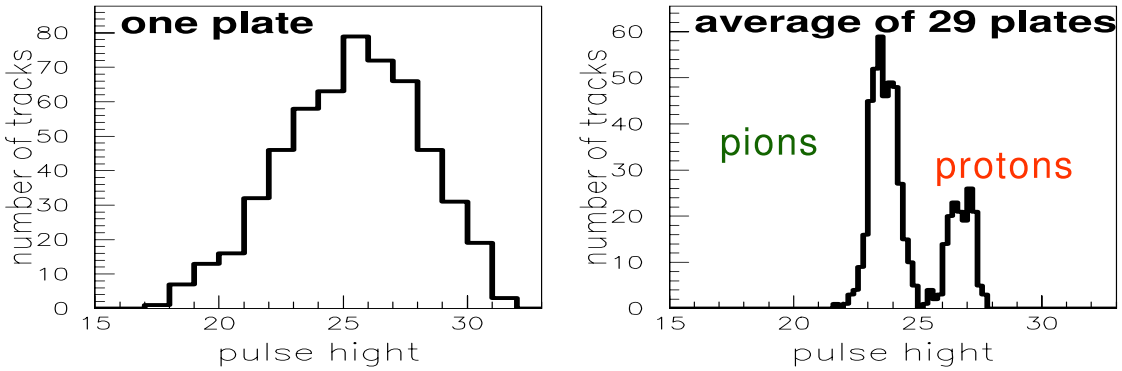

Figure 8. *Pion and proton signals in a single plate (left) and the average signal level when the particles cross 29 plates (right).*

transverse segmentation does not need to be as small, which again points towards fewer readout channels. On the other side, if the showers are large in transverse extent, this will mean that one cannot accept events that originate too close to the edge of the detector. In these cases the "fiducial volume" might be significantly lower than the actual detector volume.

3.6 Emulsion-Lead

In order to cleanly identify individual ν_τ charged current events originating from a ν_μ beam produced at CNGS, the OPERA experiment is building a sampling calorimeter made of emulsion interleaved with thin sheets of lead. Although the lead sheets are 1 mm thick and the emulsion layers are 44 μm thick, the emulsion acts as a tracking medium as well as a shower reconstruction medium. To build up enough detector mass these lead/emulsion sandwiches are packaged as 8.3 kg bricks which are then stacked to form walls of target material. The emulsion must be developed once a neutrino interaction is identified as having taken place in that brick. This is achieved by placing electronic tracking devices downstream of the target walls, which can point back to the bricks. Although the signal in one plate cannot distinguish between pions and protons, by looking at the energy loss from different tracks in a series of tracks, one can distinguish between pions and protons, as shown in Figure 8 (De Serio, M. 2005).

The signals in an emulsion detector can come from two sources. The first source, called short decays, are events where the τ is produced in the lead, travels a short distance in the lead and then decays, causing a track with a very small impact parameter compared to other tracks in the event. The second source (long decays) are events where the τ is produced, it crosses through a pair of emulsion sheets, and then decays in the next lead sheet. In this case the kink is more clearly defined. Because of the fine granularity, τ decays to both electrons and muons can be used as signal events. Figure 9 shows these two examples of decays.

The backgrounds in this detector come primarily from charm production: if the incoming neutrinos are energetic enough to undergo ν_τ charged current interactions, they are also energetic enough to produce D mesons which will also travel a short distance before decaying. These events can be eliminated, however, is by looking at the reconstructed

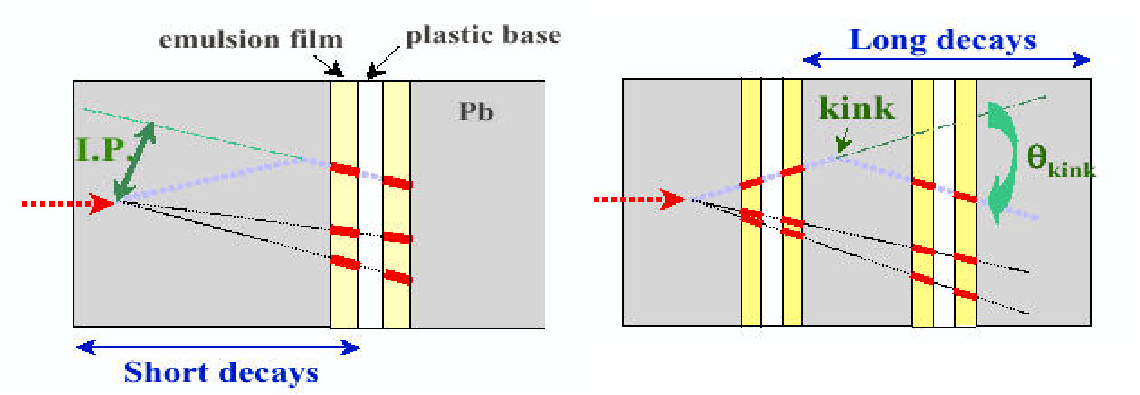

Figure 9. *Two examples of signatures that a fine grained lead emulsion detector can use to look for ν_τ charged current events through τ decays. Figure courtesy of the OPERA collaboration.*

invariant mass of the primary tracks: since these are high energy neutrino interactions in a very segmented detector, there will always be more than one track in a candidate event. The signal events will have on average a much larger invariant mass than the background events, and by cutting at an invariant mass of 3 GeV^2 99.8% of the background can be removed, at a cost of only 20% of the signal events.

Although the backgrounds are low, this detection technique is still a challenging one: the total signal detection efficiency is approximately 9.1%, split roughly evenly between the three possible decay channels: $\tau \to e$, $\tau \to \mu$ and $\tau \to$ hadrons. Nevertheless, this detector may well see more ν_τ events after 730 km of travel than the DONUT experiment saw in its short baseline experiment designed to detect ν_τ interactions in the first place!

The outstanding issues associated with this detection technique depend somewhat on what the current generation of experiments sees: if the LSND signature is really due to oscillations, then there is much more in the framework that needs to be understood, and it will be crucial to measure all of the possible transitions between different neutrino flavors. Also, if a neutrino factory of a high enough energy is in place, one could study $\nu_e \to \nu_\tau$ transitions, which would provide more information about the mixing angles θ_{23}, for example, whether or not it is above or below 45 degrees. In either case one would need to be able to identify the charge of the final state τ particle, which will be extremely challenging for all final states besides the $\tau \to \mu$ decay.

3.7 Segmented Scintillator

In order to cleanly identify ν_e charged current events originating from a ν_μ beam produced at Fermilab, the NOvA experiment is planning to build an almost entirely active detector made of plastic scintillator. Since 85% of the detector is active one might describe this not as a sampling calorimeter but more like a coarse-grained bubble chamber: the segmentation is 6 cm thick in the longitudinal direction, and 3.87 cm thick in the transverse direction. Examples of signal and background event signatures are shown in Figure 10.

The detector itself is constructed of extruded PVC tubes which are then filled with liquid scintillator, and then filled with a loop of wave-length shifting fiber which is read out

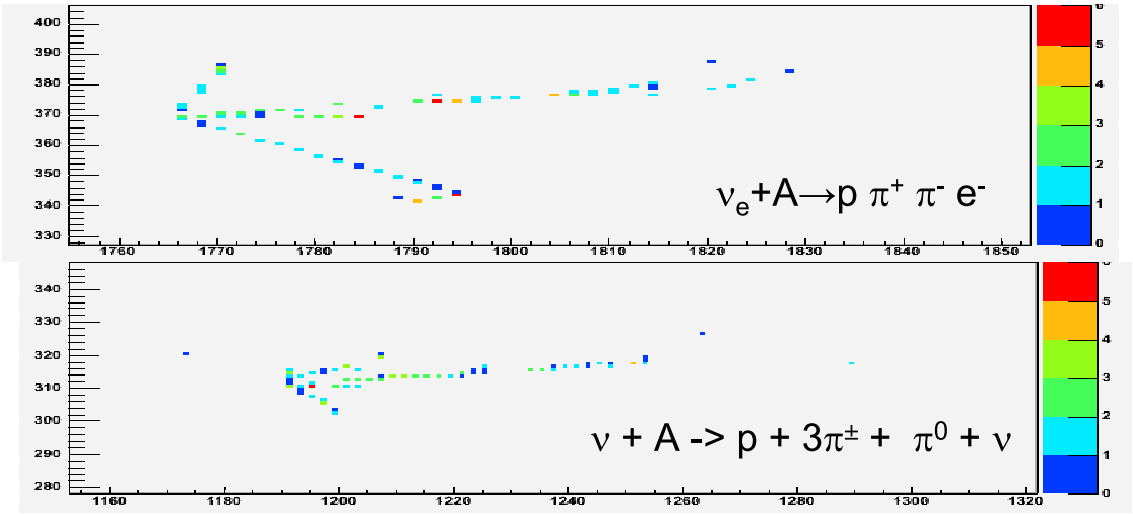

Figure 10. *Segmented Scintillator event displays for signal and background events in a $\nu_\mu \rightarrow \nu_e$ search. Event displays courtesy of the NOvA collaboration.*

at one end by avalanche photo-diodes (APD's) which are like 2-stage phototubes which are much smaller and less expensive than regular phototubes, although a little more noisy and as such must be operated at reduced temperatures.

Because this detector is built of such a low mass material and because it is a long baseline experiment looking for a small oscillation probability, the physical size of the detector is matched only by that of the Super-Kamiokande detector in Japan. The NOvA detector will weigh roughly 25 ktons, and will measure approximately 15.7 m tall by 15.7 m wide by 132 m long. Events in this detector will measure several meters long and may be one meter or more wide. Similar to the previous detectors discussed, particle identification is possible by looking at the energy loss as each particle traverses many cells of the detector. An electron track will look "fuzzy" while a muon or pion track will be much sharper. Neutral pions are often identified by the fact that the two fuzzy showers are found which point back to the same location. There is also often a several cell gap between where the neutrino interacted and either of the two photons coming from the neutral pions. In the case where there are other tracks pointing back to the primary vertex, the segmentation is a powerful method to reduce the neutral current backgrounds that would otherwise swamp the oscillation signal.

Due to the fine granularity of the NOvA detector, the energy resolution for electron neutrino charged current events is about $10\%/\sqrt{E(\mathrm{GeV})}$. For an experiment that is using a narrow-band beam, having good energy resolution is an important component of reducing the backgrounds, especially from electron neutrinos from kaon or muon decay.

The outstanding issues for this detector technology are simply associated with cost: the field of particle physics has a long history of using scintillator detectors, and the new technology associated with this detector is avalanche photo diodes. This technology choice was made to reduce the cost of the detector. The tests so far show that these detectors can operate at a low enough noise level. The biggest uncertainty is not how well this detector can reject a given background process or if the detector simulations can be made to match the detector performance, but is more related to what the cross sections for the

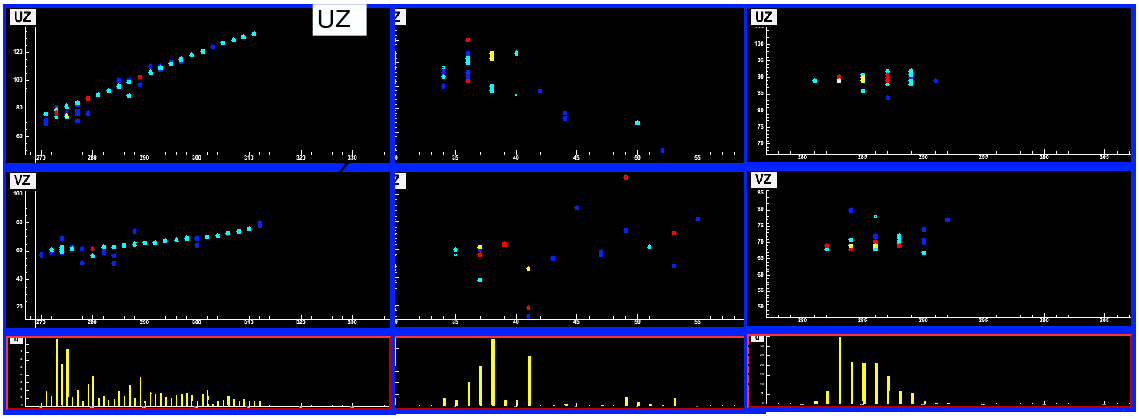
UZ
UZ
UZ
VZ
VZ

Detector Technology	Largest Mass to date (kton)	Event by Event Identification			charge identification	Ideal ν energy Range
		ν_e	ν_μ	ν_τ		
Liquid Argon TPC	0.6	yes	yes		not yet	huge
Water Cerenkov	50	yes	yes			$< 2GeV$
Emulsion/Pb/Fe	0.27	yes	yes	yes		$> 0.5GeV$
Scintillator	1	yes	yes			huge
Steel/Scintillator	5.4		yes		yes	$> 0.5GeV$

Table 6. *Summary of detector technologies currently in use or planned for future accelerator-based oscillation experiments. Although lepton charge identification has been proposed as possible in a liquid argon TPC, this has yet to be demonstrated.*

cheaper is mostly associated with understanding the minimum amount of segmentation and therefore the readout requirements. Clearly the higher the neutrino factory energy, the more coarse-grained the detector can be.

3.9 Detector Summary

The detector technologies that have been described in the previous sections are summarized in table 6. The important points to compare are what the largest mass is that has (at the time of writing) been constructed, whether or not there is event-by-event flavor discrimination, whether or not the charge of the final state lepton can be distinguished, and the energy range that each of these detector technologies is best suited. Note that there is no single detector technology which can do every possible measurement.

Although there are several technologies that have been developed for observing neutrino interactions, the demands on the next generation of detectors are large: the biggest question is how to increase the product of the detector mass and signal efficiency without similar increases in the detector cost, while keeping the background rejection high. Another point to remember is that by increasing the detector mass for accelerator-based experiments, we may gain sensitivity to other non-accelerator based physics. It is important to try to keep the functionality of these sensitive detectors high to get the most physics output from the significant investment that will be required.

4 Measuring Neutrino Oscillation Probabilities

Now that the beamlines and detectors have been described, it is worth spending some time to understand in detail how oscillation probabilities are actually measured, given a combination of these two components. Although we are currently in the "first discovery and confirmation" stage of the field of accelerator-based oscillation measurements, we will have to progress to the "precision measurements" stage in order to compare small neutrino and antineutrino probabilities and even smaller differences in probabilities. This

section will describe the strategies that are being developed to arrive at this precision measurement stage.

4.1 Overview

Recall that the number of events at a far detector (N_{far}) is related to the neutrino flux (Φ_{ν_μ}, cross section (σ_{ν_x}, detector mass (M_{far}), and oscillation probability ($P(\nu_\mu \rightarrow \nu_x)$)in the following way:

$$N_{far} = \Phi_{\nu_\mu}\sigma_{\nu_x}P(\nu_\mu \rightarrow \nu_x)\epsilon_x M_{far} + B_{far} \tag{14}$$

where ϵ_x is the detector efficiency for the signal to be detected and to pass all analysis cuts, and B_{far} is the number of background events predicted. These backgrounds can come from not only the muon neutrinos that are arriving at the far detector, but also from the intrinsic electron neutrinos in the beam or the tau neutrinos that are a result of the muon neutrinos having travelled a far distance. The background events can be expressed in the following way:

$$B_{far} = \Sigma_{i=\mu,e\tau}\Phi_{\nu_i}\sigma_{\nu_i}\epsilon_{ix}M_{far} \tag{15}$$

where ϵ_{ix} is the efficiency for identifying neutrino type i as the signal neutrino flavor x. Clearly the efficiency for detecting an electron neutrino of a given energy is the same regardless of if it's an from muon or kaon decay at the source or if it's from $\nu_\mu \rightarrow \nu_e$ oscillations.

By solving for the oscillation probability

$$P(\nu_\mu \rightarrow \nu_x) = \frac{N_{far} - B_{far}}{\Phi_{\nu_\mu}\sigma_{\nu_x}\epsilon_x M_{far}} \tag{16}$$

and then taking the derivative to look at uncertainties on that probability one arrives at the following expression:

$$\left(\frac{\delta P}{P}\right)^2 = \frac{(N_{far} + (\delta B_{far})^2)}{(\Phi_{\nu_\mu}\sigma_{\nu_x}\epsilon_x M_{far})^2} + (N_{far} - B_{far})\left(\left[\frac{\delta\phi_{\nu_\mu}}{\phi_{\nu_\mu}}\right]^2 + \left[\frac{\delta\sigma_{\nu_x}}{\sigma_{\nu_x}}\right]^2 + \left[\frac{\delta\epsilon_{\nu_x}}{\epsilon_{\nu_x}}\right]^2\right) \tag{17}$$

From this expression it is clear that there are two limits in the uncertainty on the oscillation probability: one limit where the number of signal events is comparable to the number of background events. In that case the uncertainty is dominated by the uncertainty on the background prediction and by the statistical uncertainty of the final event sample. But the other limit is in the situation where the signal events far outnumber the background events. In this case the uncertainty on the neutrino flux, the signal cross sections, and the signal efficiencies become much more important and may become larger than the statistical uncertainty.

4.2 Near Detector Justification

In order to reduce the systematic uncertainties, most oscillation experiments also place an additional detector in the same beamline, but very close to the neutrino source before the

oscillation has had a chance to occur. For an appearance experiment, the near detector will have no signal events but can put constraints on the background events if the same cuts are used to search for the signal in the near and far detector. For a disappearance experiment, the near detector can provide a constraint on the prediction of the signal events in the far detector in the absence of oscillations.

Consider an appearance experiment, where the near detector is used to look for background events: the number of events in the near detector, N_{near} is given by the following expression (assuming the same efficiency in the near and far detectors):

$$N_{near} = \Sigma_{i=\mu,e} \Phi_{\nu_i} \sigma_{\nu_i} \epsilon_{ix} M_{near} \tag{18}$$

Then, you can predict the number of events at the far detector by taking the ratio between near and far detector background expressions:

$$B_{far} = N_{near} \frac{\Sigma_{i=\mu,e,\tau} \Phi_{\nu_i} \sigma_{\nu_i} \epsilon_{ix} M_{far}}{\Sigma_{i=\mu,e} \Phi_{\nu_i} \sigma_{\nu_i} \epsilon_{ix} M_{near}} \tag{19}$$

and take advantage of the fact that detector simulations are better at predicting ratios of efficiencies and cross sections than the absolute levels. Although the claim is often made that cross sections and acceptances cancel between the near and far detector, this is only an approximation which is valid in the case for a detector with perfect energy resolution and only one process (i.e. no backgrounds).

Unfortunately, the cross sections and detector efficiencies do not cancel completely for a few reasons: first of all, because the near detector has different neutrino energy spectra than the far detector, and one must integrate the numerator and denominator both over all energies and processes. Second of all, the near detector has no ν_τ component, and because of this, the possible backgrounds from τ decay cannot be measured at all at a near detector, and furthermore, the lack of ν_μ backgrounds because of those that have oscillated to ν_τ's are also not measured. An example of how cross sections can fail to cancel using a near detector of identical capabilities is described in reference (Harris et al. 2004). Systematic uncertainties on CP violation in neutrino experiments are discussed in (Huber, Mezzetto & Schwetz 2007).

Other important differences between the near and far detector locations are the event rates and detector size. Because of cost constraints the near detector is usually much smaller than the far detector, and because of this the fiducial volume cuts will have very different effects on the near and far detectors. The close location of the near detector means that the instantaneous neutrino event rates differ from the far detector rate by a factor of 10^4 to 10^5. For neutrino beams which occur in spills lasting a few microseconds, the near detector may require much faster and therefore different electronics and data acquisition systems than the far detector. Also, for far detectors that are located deep underground, the near detectors will by definition have different cosmic ray rates than the far detectors, and hence those backgrounds will also be different.

Nevertheless, measurements at a near detector facility are a must for precision oscillation measurements, and they do put important constraints on far detector predictions. In this next section we will describe briefly the near detector designs for previous, current, and future neutrino oscillation experiments.

4.3 Near Detector Strategies

There are two different strategies for designing near detectors for oscillation experiments: one strategy is to build a near detector that is as identical as possible to the far detector, given the constraints listed above. Since the far detector is by definition only as segmented as one can afford, this means that with this strategy the near detector is also only as segmented as the far detector. So once similar kinds of cuts are made, one cannot distinguish how much of the "near detector background events" come from the various sources of backgrounds. For ν_e oscillation experiments, the three sources (neutral currents, ν_μ charged currents, and intrinsic ν_e's in the beam) all have very different far detector to near detector extrapolations, so the far detector prediction will suffer from uncertainties in the various cross sections that make up the near detector signal rates.

The second strategy is to have a near detector that is much more fine-grained and gives much more information than the far detector, and then rely on Monte Carlo simulations to predict the far detector signal efficiencies. In this way the near detector measures the product of the flux and cross sections well. The uncertainty arises from the predictions on the efficiencies of the far detector.

4.3.1 K2K

The K2K experiment used the 50 kton Super-Kamiokande Water Cerenkov detector for the far detector (Nakahata et al. 1999), and used several near detectors including a 1 kton Water Cerenkov detector at a nearby location (Suzuki et al. 2000, Ishii et al. 2002, Maesaka 2003). Because the near water Cerenkov detector was much smaller the events were on average much closer to the phototube wall than at the far detector, and understanding the efficiency as a function of distance from that wall was extremely important. To understand the cross sections and the population of events that would be below Cerenkov threshold, the K2K experiment also had a scintillating fiber tracker with a 6 ton fiducial mass water target, as well as a 9.38 ton fiducial mass fully active scintillator tracker detector. Finally, because only very low energy muons would range out in any of the upstream near detectors, there was also a muon range detector of 330 tons of fiducial mass. This last detector was large enough in transverse dimensions to see the high energy muons and measure the direction of the neutrino beam that produced those high energy muons after interacting in the steel.

4.3.2 T2K

The T2K experiment, which will also use the Super-Kamiokande Water Cerenkov detector as a far detector, has a slightly different program of near detectors planned(Itow et al. 2001). There are two planned locations for near detectors: one location is at 280 m from the proton target, and the other is at 2 km from the proton target. The 280 m detector location will have two neutrino detectors: one that is located on the beamline axis whose function is strictly to measure the beam direction using iron and scintillator stacks in a grid of locations. The other 280 m detector will be a fine-grained detector that has two detector technologies: one a water target instrumented with electromagnetic calorimetry to understand sources of electrons and photons in an off axis neutrino beam, and the second region will be a TPC combined with fine grained detectors, also with

a water target, to measure the secondary particle energy spectra from neutrino-water interactions.

At the 2km location there are plans to use both a water Cerenkov detector and a liquid argon TPC, followed by a muon range detector. This more downstream site has a muon and electron neutrino flux that is much closer to the far detector flux at least before oscillations, and should be extremely useful for precise muon neutrino disappearance measurements.

4.3.3 MINOS

The MINOS experiment (Adamson et al. 2006), which uses a 5.4 kton steel scintillator far detector that is 8 m in transverse dimension to the beam axis, has a 1 kton near detector that is also steel scintillator with the same longitudinal segmentation for the target area of the detector, although it measures roughly 3.8 m $\times$ 4.8 m in transverse size. The downstream region of the MINOS near detector is instrumented with scintillator only once for every five planes of steel and is used as a muon spectrometer. Because of the very high event rate the MINOS detector uses much faster electronics to get continuous sampling in the spill, which it must do in order to untangle the many events that occur in the MINOS near detector for every 10 microsecond spill.

4.3.4 NOvA

The NOvA experiment, which will use a 25 kton segmented scintillator detector for its far detector, uses an almost identical near detector but one that is significantly smaller in the transverse direction (Ayres et al. 2004). The far detector measures roughly 16 m $\times$ 16 m, while the near detector measures 4.1 m $\times$ 2.1 m Because the near detector is constrained in size based on the fact that it will be in an underground enclosure, the muon spectrometer region of this detector will be made of steel and scintillator planes rather than only scintillator, but the total detector size will be long enough to contain 2 GeV muons that enter the upstream region of the detector. Because the decay pipe for the NOvA experiment is so long and the near detector is so near to the end of the decay pipe, there is a large difference between the near and far detector spectrum, so the NOvA experiment is considering making measurements at several off axis angles, not only the off axis angle that is identical to the far detector. This would help reduce the uncertainties on the far detector prediction since they will have a few slightly different near detector spectra to compare.

4.4 Muon Neutrino Disappearance Measurements

According to the atmospheric neutrino measurements, the mixing angle between muon neutrinos and tau neutrinos is near or at maximal. This means that the disappearance phenomenon is very large which permits statistically a very precise measurement of the mass difference between the two neutrino species, given a well-understood muon neutrino beam. In order to measure the mass difference one must measure the oscillation probability versus neutrino energy for a given distance or alternatively for the same energy at several distances. The challenge is to measure the incoming neutrino energy as accurately

as required. How well do we really know what the incoming neutrino energy is? We can measure the final state particle energies, but this might not be the whole story.

Quasi-elastic events have a great feature where you can measure the lepton angle θ_ℓ and momentum (p_ℓ) and derive the neutrino energy (E_ν) if you assume a quasi-elastic interaction off a proton. In this case the neutrino energy is given by the following expression:

$$E_\nu = \frac{m_N E_\ell - m_\ell^2/2}{m_N - E_\ell + p_\ell \cos\theta_\ell} \tag{20}$$

where m_N is the nucleon mass. But what happens when there is an interaction with a higher hadronic mass? If you miss the other final state particles, you will reconstruct a lower energy than what the original neutrino energy was. So you need to know your detector's ability to see those other particles. You also need to know how often those other particles are produced. This is much harder and goes back to knowing cross sections and differential distributions of the secondary lepton. So the dominant uncertainty in the energy measurement for a water Cerenkov detector is the ratio of quasi-elastic to non-quasi-elastic cross sections. This is the justification for building several near detectors, at least one of which has pion and proton detection well below the Cerenkov threshold.

Fully active detectors have another problem: they have lower detection thresholds so that is an advantage, but on the other hand they still have to deal with the nuclear environment. The center of a nucleus is a very dense place, and there is a substantial probability that a pion produced there will be absorbed or at least lose a lot of energy as it leaves the nucleus. If no particles lost energy in this way, you don't have to worry so much about how many final state particles, assuming your detector is linear: if your detector produces ten 1 GeV pion or three 3 GeV pions the detector energy measured might be the same. But if the probability of absorbing the 300 MeV pions is 5 times the probability of absorbing the 1 GeV pion, then you do care how many times a neutrino makes the 300 MeV pions compared to the 1 GeV pions.

Another important concern in a muon neutrino disappearance measurement comes from knowing the neutral current background accurately. Since the mixing angle for disappearance is near maximal, at the oscillation minimum most of the events may well be neutral current events which have been mis-identified as charged current events. The uncertainty on that contamination is very difficult to constrain at the near detector because the charged current fraction is so much higher at the near detector, and only the tails of the neutral current events will contaminate the charged current event selection. Measuring those tails when they are even more hidden by the near detector charged current sample is difficult.

One technique that the MINOS experiment uses to better constrain their far detector predictions is to look at the near detector data in several different beam configurations. The NuMI beamline was designed specifically to accommodate different target locations relative to the positions of the two horns, and the movement from one target location to another was possible by remote operations and only took a few minutes. Because of this the MINOS experiment took several weeks of data in conditions that were not optimal for seeing an oscillation signal at the far detector, but could be used as tests of the experiments understanding of the near detector events. The data taken in some of these configurations are shown in Figure 12. By moving the neutrino target back and forth with respect to the horn location, they select different momentum for the "tune"

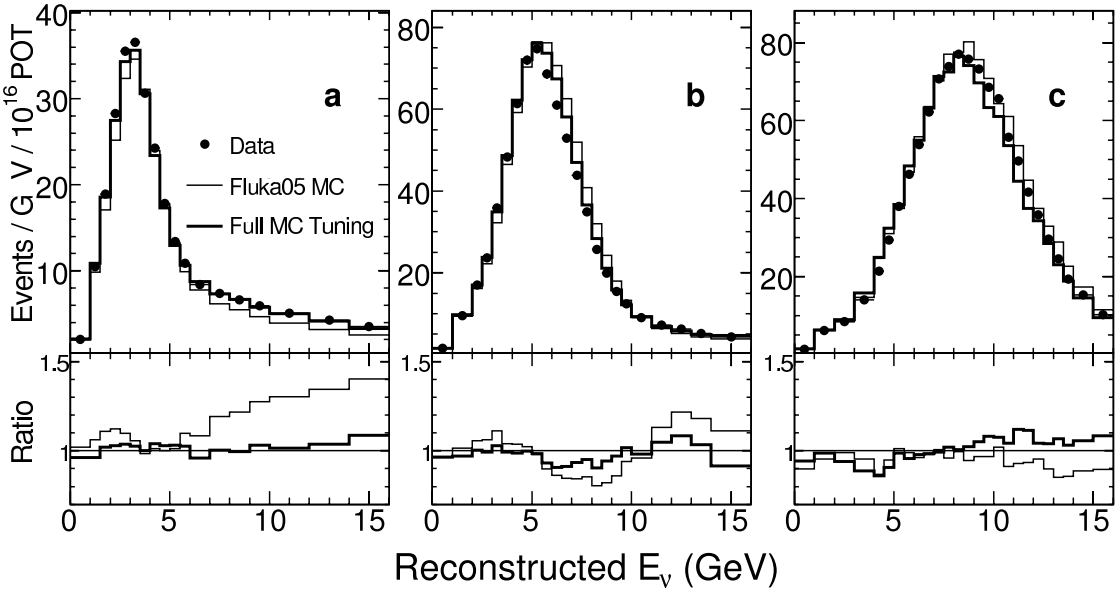

Figure 12. *MINOS near detector events for different beamline configurations, as described in the text.*

momentum of the beam which results in different near (and far) detector neutrino energy spectra. These events will all have different neutral current and charged current fractions, which can better constrain the model than only one target position data. Similarly, they also took data at several different horn currents: this means that although the event rate coming from pions that went through the inside of the inner conductor does not change, the focused peak can be dramatically reduced. This also lowers the number of signal events in the low energy charged current sample and so the ratio of neutral to charged currents can be closer to that expected in the case of oscillations at the far detector.

4.5 Electron Neutrino Appearance in a Muon Neutrino Beam

The most important information that accelerator-based experiments can tell us about neutrino oscillations will come from comparisons of neutrino and antineutrino oscillations between muon and electron neutrinos. Measurements of CP violation and measurements of the neutrino mass hierarchy simply cannot be done by any other kind of experiment. Therefore it is important that we understand just how to get to precision measurements of these quantities, and what the challenges are. Unfortunately there are several different backgrounds that arise in a conventional neutrino beam when one is searching for electron neutrino appearance.

The first background, as mentioned above, comes from electron neutrinos produced at the accelerator itself. These are produced in muon and kaon decays in the beamline. Event by event these neutrinos will look in every way like the signal neutrinos, the only difference is that their total energy distribution will be very different from that of the signal neutrinos from muon neutrino oscillations. The second background, shown at the left in Figure 13 comes from neutral current events that contain neutral pions, where one or more of the photons from the pion decay is mis-reconstructed as a single electron in the far detector. Again the measured neutrino (and "electron candidate") energy

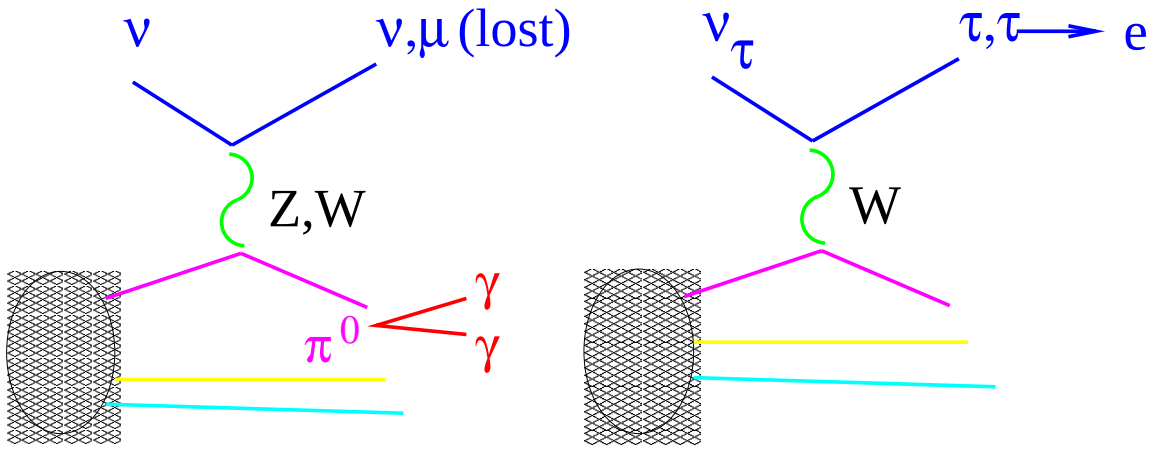

Figure 13. *Feynman diagrams for backgrounds to electron neutrino searches in muon neutrino beams.*

distributions will be different from the signal neutrinos, since the neutral current visible energy spectrum is steeply falling.

The third background, also shown at the left in Figure 13 comes from ν_μ charged current events where the outgoing muon is so low in energy that a neutral pion again from the hadronic shower is mis-reconstructed as a single electron and is tagged as the leading lepton in the event. This background is particularly dangerous not because it is large, but because due to $\nu_\mu \rightarrow \nu_\tau$ oscillations, the background energy distribution from this source will be extremely different between the near and far detectors.

The last background, shown at the right in Figure 13 is relevant only for higher energy neutrino beams, comes from ν_τ charged current events where the τ decays into an electron. The neutrino and lepton energy distributions will be different between signal and background events, but the challenge here is that this background cannot be measured at all at a near detector since by definition the τ neutrinos have not yet begun to appear.

The initial relative levels of these four backgrounds differ depending on what detector technology is employed, and depending on how optimized the beamline has been for the ratio between muon and electron neutrino production. Table 7 lists the number of events for a "standard exposure" for many of the experiments that have been described in this article, for an optimized analysis. Although the intrinsic ν_e fractions of the different beamlines are all different (see Table 3) it is clear that the experiments optimized for ν_e appearance have a background dominated by the intrinsic ν_e component in the beamline. The signal rates shown assume that $\sin^2\theta_{13} = 0.1$ and that $\delta = 0$, and the NOvA signal assumes that the neutrino mass hierarchy is the normal one. All these signals assume slightly different δm^2 values but within $2.5 - 3 \times 10^{-3} eV^2$.

5 Summary

Although the field of neutrino oscillations was started by measurements of naturally occurring sources of neutrinos, namely the sun and the atmosphere, the ultimate steps that need to be taken depend on accelerator-based sources of neutrinos. The search for CP violation in the lepton sector and a determination of the neutrino mass hierarchy may

Experiment	Background					Signal	Figure
	$\nu_\mu CC$	NC	ν_e	ν_τ CC	Total		of Merit
K2K (Yamamoto et al. 2006)	0	1.3	0.4	0	1.7	1	0.6
MINOS (Smith 2006)	5.6	39	8.7	4.7	58	29.1	3.1
OPERA (Komatsu et al. 2003)	1	5.2	18	4.5	28.7	10	1.6
T2K (Itow et al. 2001)	1.8	9.3	11.1	0	22.2	103	9
NOvA (Ayres et al. 2004)	0.5	7	11	0	18.5	148	11.5

Table 7. *Table describing the signal and background rates for a typical exposure for long baseline ν_e appearance search. The "figure of merit" is defined as the signal divided by the square root of the total number of signal and background events expected.*

ultimately require extremely powerful neutrino beams and massive detectors that are beyond what is currently planned. How challenging these measurements will be depends on the size of the last unmeasured mixing angle in the leptonic mixing matrix.

Because of the inherent contamination in conventional neutrino beams, new beamline strategies such as beta beams or neutrino factories are being investigated. Similarly, because of the difficulty of distinguishing between neutral pions made in neutral current interactions and electrons in electron neutrino charged current interactions, new detector strategies such as liquid argon are being investigated. Both examples offer potentially large breakthroughs in the level of backgrounds that would be seen in these future experiments.

Finally, it will take more than massive detectors and powerful beamlines to make these measurements. The goals of discovering CP violation and mass hierarchy will be achieved by comparing the differences of oscillation probabilities that are already limited to being on the order of a few percent. To make these comparisons we will need a detailed understanding of how the neutrino beam is produced, and how the neutrinos themselves interact in these massive detectors. The field of oscillations was born from two very surprising results, and we should not presume to know the origin of the next surprise.

Bibliography

Adamson, P. et al. (2006), 'The MINOS calibration detector', *Nucl. Instrum. Meth.* **A556**, 119–133.

Aguilar-Arevalo, A. A. et al. (2007), 'A search for electron neutrino appearance at the $\Delta m^2 \sim 1$ eV^2 scale', *Phys. Rev. Lett.* **98**, 231801.

Aliu, E. et al. (2005), 'Evidence for muon neutrino oscillation in an accelerator-based experiment', *Phys. Rev. Lett.* **94**, 081802.

Apollonio, M. et al. (2003), 'Search for neutrino oscillations on a long base-line at the CHOOZ nuclear power station', *Eur. Phys. J.* **C27**, 331–374.

Astier, P. et al. (2001), 'Final NOMAD results on $\nu_\mu \to \nu_\tau$ and $\nu_e \to \nu_\tau$ oscillations including a new search for ν_τ appearance using hadronic tau decays', *Nucl. Phys.* **B611**, 3–39.

Athanassopoulos, C. et al. (1996), 'Evidence for $\bar{\nu_\mu} \to \bar{\nu_e}$ oscillation from the LSND experiment at the Los Alamos Meson Physics Facility', *Phys. Rev. Lett.* **77**, 3082–3085.

Ayres, D. S. et al. (2004), 'NOvA proposal to build a 30-kiloton off-axis detector to study neutrino oscillations in the Fermilab NuMI beamline', *hep-ex/0503053* .

Burguet-Castell, J., Casper, D., Gomez-Cadenas, J. J., Hernandez, P. & Sanchez, F. (2004), 'Neutrino oscillation physics with a higher gamma beta- beam', *Nucl. Phys.* **B695**, 217–240.

De Serio, M. (2005), The OPERA experiment, Weak Interations and Neutrinos, CERN.

Eskut, E. et al. (2007), 'Final results on $\nu_\mu \to \nu_\tau$ oscillation from the CHORUS experiment', *arXiv:0710.3361 [hep-ex]* .

Fisher, P., Kayser, B. & McFarland, K. S. (1999), 'Neutrino mass and oscillation', *Ann. Rev. Nucl. Part. Sci.* **49**, 481–528.

Fitton, M. (2006), Design and computational fluid dynamic analysis of the T2K target, Neutrino Beams and Instrumentation, CERN.

Fukuda, Y. et al. (1998*a*), 'Evidence for oscillation of atmospheric neutrinos', *Phys. Rev. Lett.* **81**, 1562–1567.

Fukuda, Y. et al. (1998*b*), 'Measurements of the solar neutrino flux from Super-Kamiokande's first 300 days', *Phys. Rev. Lett.* **81**, 1158–1162.

Geer, S. (1998), 'Neutrino beams from muon storage rings: Characteristics and physics potential', *Phys. Rev.* **D57**, 6989–6997.

Harris, D. A. et al. (2004), 'Neutrino scattering uncertainties and their role in long baseline oscillation experiments', *hep-ex/0410005* .

Huber, P., Mezzetto, M. & Schwetz, T. (2007), 'On the impact of systematical uncertainties for the CP violation measurement in superbeam experiments', *arXiv:0711.2950 [hep-ph]* .

Ishii, T. et al. (2002), 'Near muon range detector for the K2K experiment: Construction and performance', *Nucl. Instrum. Meth.* **A482**, 244–253.

Itow, Y. et al. (2001), 'The JHF-Kamioka neutrino project', *hep-ex/0106019* .

Kobayashi, M. & Maskawa, T. (1973), 'CP Violation in the renormalizable theory of weak interaction', *Prog. Theor. Phys.* **49**, 652–657.

Komatsu, M. et al. (2003), 'Sensitivity to theta(13) of the CERN to Gran Sasso neutrino beam', *J. Phys.* **G29**, 443.

Kopp, S. E. (2007), 'Accelerator neutrino beams', *Phys. Rept.* **439**, 101–159.

Kuno, Y. (2007), This volume.

Maesaka, H. (2003), 'The K2K SciBar detector'. Prepared for KEK - RCNP International School and Miniworkshop for Scintillating Crystals and their Applications in Particle and Nuclear Physics, Tsukuba, Japan, 17-18 Nov 2003.

Michael, D. G. et al. (2006), 'Observation of muon neutrino disappearance with the MINOS detectors and the NuMI neutrino beam', *Phys. Rev. Lett.* **97**, 191801.

Nakadaira, T. (2005), 'J-PARC neutrino beam line and target development', *Nucl. Phys. Proc. Suppl.* **149**, 303–305.

Nakahata, M. et al. (1999), 'Calibration of Super-Kamiokande using an electron linac', *Nucl. Instrum. Meth.* **A421**, 113–129.

Rubbia, A. (2005), Concepts and R&D for very large liquid argon time project chambers, International Neutrino Factory and Superbeam Scoping Study Meeting, CERN.

Shiozawa, M. (1999), 'Reconstruction algorithms in the Super-Kamiokande large water Cherenkov detector', *Nucl. Instrum. Meth.* **A433**, 240–246.

Smith, C. (2006), MINOS results from the first year of NuMI operations, Fermilab Joint Theoretical and Experimental Seminar, FERMILAB.

Suzuki, A. et al. (2000), 'Design, construction, and operation of SciFi tracking detector for K2K experiment', *Nucl. Instrum. Meth.* **A453**, 165–176.

Yamamoto, S. et al. (2006), 'An improved search for $\nu_\mu \to \nu_e$ oscillation in a long-baseline accelerator experiment', *Phys. Rev. Lett.* **96**, 181801.

Yao, W.M. et al. (2006), 'Particle Data Group', *Journal of Physics G* **33**, 1.

Zucchelli, P. (2002), 'A novel concept for a $\bar{\nu_e}/\nu_e$ neutrino factory: The beta beam', *Phys. Lett.* **B532**, 166–172.